Study on Residual Stresses in Unidirectional Flax Fiber/Vinyl Ester Composites by XRD Technique

Shanshan Huo and Chad A. Ulven*

Mechanical Engineering Department, North Dakota State University, Fargo, ND 58105, USA

ABSTRACT: The development of flax fiber reinforced polymer composites with improved properties has been increasingly studied by many researchers because of their sustainability. However, the effects of thermal residual stresses on the interfacial properties of flax composites have not been evaluated or very well understood. In this study, the thermal properties of flax, vinyl ester matrices and their composites were accessed by different techniques, including thermomechanical analyzer, dynamic mechanical analyzer, and X-ray diffraction combined with aluminum particles. The effects of thermal properties of flax fibers and vinyl ester resin systems on the mechanical properties of their biocomposites were studied. The theory of modifying the thermal properties of flax and vinyl ester to improve the interfacial adhesion between them has been proven by the study of the thermal residual stresses in their composites.

KEYWORDS: Residual stress, X-ray diffraction, biocomposites, interfacial properties

1 INTRODUCTION

Bast fibers are one of the most widely used types of cellulosic natural fibers for producing biocomposites [1]. Flax fibers, a specific type of bast fiber, have historically been used as reinforcements in composites because they offer competitive advantages, including environmental and economic benefits, over mineral-based reinforcing fibers. However, because of the hydrophilicity of flax fibers and the hydrophobicity of most polymer matrices, poor interfacial bonding reduces the mechanical performance of flax thermoset biocomposites. To improve the interfacial properties of flax biocomposites, different physical, chemical, or physicochemical modifications have been applied to flax fibers [2–7]. These surface modifications can reduce non-cellulose components, decrease the hydrophilicity of flax fibers, and improve chemical bonding or entanglement between flax fiber and polymer matrices.

On the other hand, the polymer matrix can also be modified to improve the adhesion between fibers and matrices. In a previous study [8], acrylic resin (AR) was used to manipulate vinyl ester (VE) system to improve the mechanical performance of flax/VE composites.

The AR brings more carbonyl groups to VE systems, increases the polarity of the matrix system and as a result improves the interfacial properties of flax/VE with AR composites [9].

In addition, the structure of flax fiber is more complex than that of mineral or synthetic fibers [10], which renders most of the traditional mechanical tests for the evaluation of transverse direction for interfacial properties of flax biocomposites invalid. Therefore, a nondestructive method to evaluate the interfacial properties of natural fiber composites is needed. Moreover, the effects of the thermal properties of both flax and VE system on the mechanical properties of flax/VE composite have not been studied.

The thermal residual stresses at the interface between fibers and matrix and inside of the resin and fiber are a result of chemical shrinkage and thermal cooling contraction [11–13]. These internal thermal residual stresses affect the quality of the interfacial interaction of the fiber reinforced composites [14–16]. The interface condition can affect the toughness, stiffness and strength of the composites [17]. There are numerous methods that have been developed to determine the residual stresses in the fiber reinforced polymer composites. X-ray diffraction combined with embedded metallic particles is usually used to measure the deformation induced by residual strains in amorphous polymer composites. The embedded sensor can

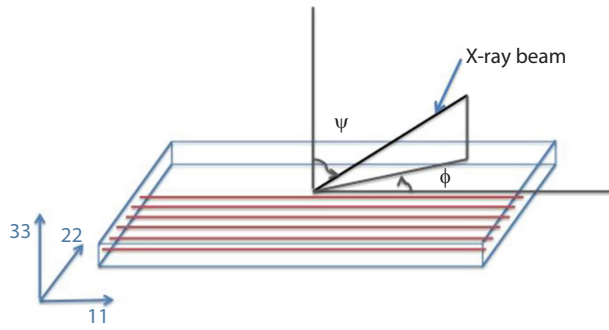*Corresponding author*: chad.ulven@ndsu.edu

Figure 1 The diffraction plane and the coordinates of the specimen.

be aluminum, copper, silver, or nickel. Aluminum (Al) particles, which are spherical or nearly spherical, have been found to provide the highest accuracy [18].

Embedded particles can show a change in the diffraction peak angle due to the residual strains induced by the polymer. The crystal lattice spacing can be calculated using Bragg's law. There are two rectilinear coordinate systems used in X-ray diffraction stress measurements [19]. One is the laboratory coordinate system (principal system), which consists of the axes with respect to which diffraction measurements are made. The other one is the sample coordinate system (normal system) and the angle ϕ and ψ defined in Figure 1. The difference between $d_{\phi\psi}$, the value of d in the stressed sample and measured for the plane whose normal is at angle ϕ and ψ, and the value of d_0 for the unstressed state, is related by Equation 1:

$$\varepsilon_{\phi\psi} = (d_{\phi\psi}-d_0)/d_0 \tag{1}$$

d_0 is the stress-free lattice spacing, which is measured from the filler powder. Knowing the X-ray elastic constant (XEC) S_1^{hkl} and $(1/2)S_2^{hkl}$, the strain measured in the direction by ϕ and ψ is given, in terms of the principal stresses, by Equation 2.

$$\varepsilon_{\phi\psi} = (d_{\phi\psi}-d_0)/d_0 = (1/2)\,S_2^{hkl}(\sigma_{11}cos^2\phi\,sin^2\psi + \sigma_{22}sin^2\phi sin^2\psi + \varepsilon_{33}cos^2\psi)+ S_1^{hkl}(\sigma_{11}+\sigma_{22}+\sigma_{33}) \tag{2}$$

Dölle [20] describes a method to calculate XEC using single crystal elastic constants S_{11}, S_{12}, and S_{66} for cubic symmetry. By using the Voigt and Reuss models, the average XEC values (Voigt and Reuss) for Al (422) can be calculated [21]. The strain components ε_{ij} (i, j = 1, 2, 3) in the specimen coordinate system can be calculated by Equation 3:

$$\varepsilon_{\phi\psi} = (d_{\phi\psi}-d_0)/d_0 = \varepsilon_{11}cos^2\phi sin^2\psi+\varepsilon_{12}sin2\phi sin^2\psi+\varepsilon_{22}sin^2\phi sin^2\psi+\varepsilon_{33}cos^2\psi+\varepsilon_{13}cos\phi sin2\psi +\varepsilon_{23}sin\phi sin2\psi \tag{3}$$

ε_{33} is calculated by Equation 4:

$$\varepsilon_{33}=(\varepsilon_{\phi = 0,\psi = 0} +\varepsilon_{\phi = 90,\psi = 0})/2 \tag{4}$$

ε_{11} and ε_{22} are obtained from the slopes of the $sin^2\psi$ plots at ϕ = 0° and 90°. The stresses on the surface of Al particles can then be calculated from the strain by using Hooke's law, assuming the system is isotropic.

In this study, alkaline treatment was chosen to clean flax fiber to reduce the effects of non-cellulosic chemicals. Different amounts of AR were added into VE resin system to improve the mechanical performance of flax/VE composites, as previously shown [8,9]. Coefficient of linear thermal expansion (CLTE) of alkaline treated flax was evaluated by thermomechanical analyzer (TMA), and CLTEs of different VE systems were assessed by dynamic mechanical analyzer (DMA). The deformation caused by thermal residual stresses inside the flax/VE composites was measured by X-ray diffraction. The effects of thermal residual stresses in flax/VE on their mechanical properties were then discussed.

2 EXPERIMENTAL PROCEDURE

2.1 Materials

Unidirectional Chinese flax was water retted with the minimum mechanical handling from Harbin, China. The flax fiber was uncut, natural colored, and from a stalk with a density of approximately 1.42 g/cm³. Ethanol (95%) and sodium hydroxide (99.9%) were obtained from Sigma-Aldrich Co. The resin system used for all grades was a VE resin Hydropel® R037-YDF-40 from AOC Resins, and 2-Butanone peroxide (Luperox® DDM-9) solution was used as the curing initiator, obtained from Sigma-Aldrich Co. Acronal® 700 L AR, which is a copolymer of n-butyl acrylate and vinyl isobutyl ether, was obtained from BASF Aktiengesellschaft, Ludwigshafen, Germany,.

2.2 Surface Treatment

2.2.1 Alkaline Treatment

The flax fibers as received were immersed into 500 mL of 10 g/L sodium hydroxide ethanol solution at 78 °C for 2 h. The treated fibers were washed with distilled water until no color was left in the water (pH was about 7, which was measured by pH paper). Then the fibers were dried in an oven for 24 h at 80 °C.

2.3 Composite Processing

2.3.1 Composite Panels for Mechanical Testing

Composite panels of flax/VE were fabricated using a modified form of vacuum assisted resin transfer

molding (VARTM) [8]. A caul plate was used underneath the vacuum bag to provide a uniform cross-sectional area. This also created a test specimen with a smooth surface on both sides. In order to obtain similar fiber volume fractions, the VARTM process was aided by compressing the vacuumed flax with 2 metric ton force. The manually aligned unidirectional fibers showed a deviation of 0° to 10° with respect to the lay-up direction.

To improve the interaction between flax fibers and VE, AR was also added to the VE resin. AR is a highly viscous liquid that is used particularly in combination with cellulose nitrate. The fibers/VE with 1 wt% AR composites were also processed by the modified VARTM.

2.3.2 Composite Panels for X-ray Diffraction

Aluminum (Al) powder was dispersed into absolute ethanol by high shear stirring to form a homogenous slurry, in which a concentration of 0.5 wt% 5 ~ 6 g NaOH/ethanol treated flax was quickly put into the slurry and taken out under the nitrogen atmosphere and then the fiber was dried in the nitrogen atmosphere at room temperature for 24 h. The composite samples were manufactured by the modified VARTM with 1 metric ton force under a nitrogen atmosphere.

2.4 Characterization

2.4.1 Thermal Properties of Flax Fiber

The CLTE of the treated flax was measured by a TA Instruments 2940 TMA. TMA measured the displacement in the cross section of the treated flax fibers as a function of temperature under a controlled atmosphere. A small bundle of fibers with combed lineup was placed on the tip of the probe and the temperature was increased from 25 °C to 150 °C by 10 °C/min. Three measurements were applied to calculate the average of the CTE of the cross-section area.

2.4.2 Thermal Properties of VE Systems

The CLTEs of VE and VE with AR were measured by a TA Instruments Q800 DMA using tension film fixture. Four rectangular specimens with dimensions of 15 × 7.8 × 2.69 mm for both neat VE and VE with 1% AR were prepared. The measurements were performed from 30 to 150 °C at a heating rate of 5 °C/min. In addition, the T_gs of both VE systems were evaluated by DMA with the dual cantilever fixtures. Four rectangular specimens (dimension: 46 × 10.6 × 3.71 mm) for each resin system were measured from 30 to 180 °C with a heating rate of 3 °C/min. The shrinkage after curing of VE and modified VE with AR was evaluated by measuring the volume changes before and after the curing. The liquid VE resin mixture was put into a square Al mold and the width, length and height of the liquid were measured. Then, the geometries of the cured VE were measured to calculate the volume changes after curing.

2.4.3 Mechanical Properties

Interlaminar shear strengths (ILSS) were assessed using short-beam strength tests according to ASTM D2344. Short-beam shear tests were carried out in displacement control at a rate of approximately 1 mm/min on an Instron 5567 load frame with a 2 kN load cell. Five specimens for each sample were tested.

Tensile testing was performed according to ASTM D3039 with a five-specimen sample set using an Instron 5567 load frame. The speed of the crosshead was 1.0 mm/min. Each test was performed until tensile failure occurred. The tensile modulus of each specimen was recalculated by the slope of stress-strain plot in the linear region, where the displacement is measured by an extensometer.

2.4.4 X-ray Diffraction

The treated flax/VE (with/without AR) with Al powder composites were marked at six angles (0°, 30°, 45°, 90°, 120° and 135°), in which the longitudinal directional of the fiber is the direction of 0°. The XRD spectra of different angles were captured using a Philips X'PERT MPD X-ray powder diffractometer. The XRD diffraction conditions are shown in Table 1. The radiation is generated from Cu-K$_α$, and λ of K-α1 is 1.54060 Å and λ of K-α2 is 1.54443 Å. The scan was started at the position (2θ) of 136.01° and stopped at the position (2θ) of 138.99° at room temperature, in which the step (2θ) size is 0.0200°. Peak separation of Al at (422) was carried out using least squares fitting by assigning Gaussian functions. The original Al powder was scanned using the same procedure.

Figure 2 lists the experiments conducted on flax fiber, VE resin systems and their composites in this study. All these tests examine the physical factors pertaining to the mechanical performance of the flax/VE composites, which help to evaluate the effects of thermal residual stresses on the interfacial properties of flax.

Table 1 X-ray diffraction conditions.

Radiation	Cu Kα$_1$, λ = 1.54060 Å
Reflection (hkl)	422
2θ range (°)	136 ~ 139
Step size (°)	0.0200
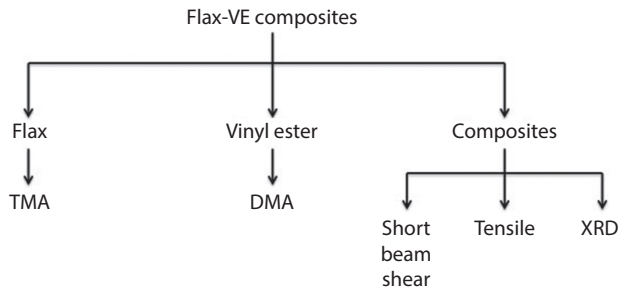
Figure 2 Flow diagram of the experimental study.

Figure 3 The CLTE curve of the treated flax measured by TMA.

3 RESULTS AND DISCUSSION

3.1 Thermal Analysis

3.1.1 Coefficient of Linear Thermal Expansion of Treated Flax

The CLTE of treated flax fiber was measured by TMA and used as the CLTE of the cross-section area α_T. Figure 3 shows the test curve of the treated flax. The contraction in the region lower than 100 °C in the curve is close to linear and the region above 110 °C drops dramatically. However, the temperature during the curing of the composite was normally below 80 °C in this study, so the region from 40 °C to 80 °C was used to calculate α_T of the treated flax. CLTE (α_T) of the treated flax was found to be −299.1 ± 87.1 µm/m °C. The mismatching of CLTEs between flax and VE system can introduce the thermal residual stresses to the composites during the curing, which can influence the interfacial properties of the composites. The CLTE of flax in the transverse direction was used to calculate the thermal residual stresses in the composites.

3.1.2 Thermal Properties of VE Systems

The shrinkages after curing of neat VE and VE with 1% AR are presented in Table 2. The shrinkage of neat VE is the lowest and its volume after curing decreases approximately 10%. On the other hand, the shrinkage of VE with 1% AR has the highest volume change after curing. The shrinkages after curing are related to the thermal expansion of the VE system and the thermal residual stresses generated by curing in the matrix. The difference in shrinkage among the three VE systems indicates that AR additive changes CLTEs of the VE systems.

The CLTEs of neat VE and VE with 1% AR in the region between 40 °C to 80 °C listed in Table 3 were measured by DMA. The thermal expansion of VE is not linear because there are two phases in the VE structure, which have different CLTEs. In this study, the composites are cured at room temperature and,
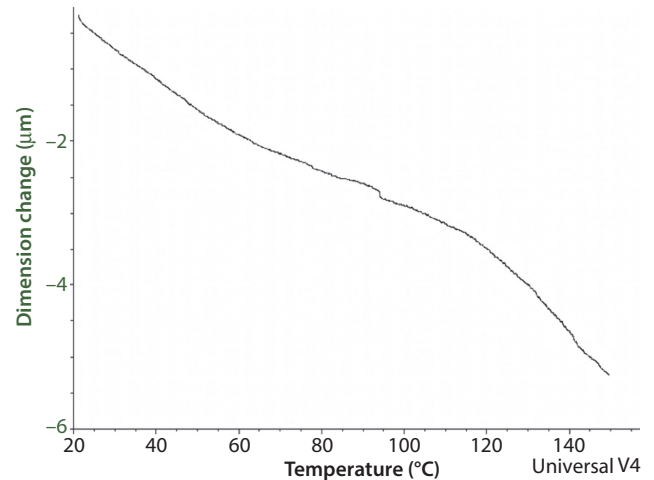
Table 2 The shrinkages after curing of different VE systems.

Sample	Volume before Curing (mm³)	Volume after Curing (mm³)	Shrinkage (%)
Neat VE	142912.73	128563.86	10.04 ± 0.37
VE with 1% AR	146178.24	127575.88	12.73 ± 0.17

Table 3 The linear coefficients of thermal expansion of VE systems.

Sample	CLTE (40 °C to 80 °C) µm/m °C
Neat VE	19.66 ± 0.89
VE with 1% AR	21.46 ± 0.16

during the curing, the temperature of the panel rises slightly. However, the temperature of the curing panel is lower than 80 °C. Thus, CLTEs of VE systems are evaluated from the region under 80 °C. CLTE of modified VE system is higher than neat VE, which indicates that AR added into VE system increases the sensitivity to the temperature. Meanwhile, the DMA plot of modified system is more linear than neat VE, which is because AR reduces the separation of the two phases in VE and helps the two regions mix together. The effects of CLTEs of different VE systems on the interfacial properties of flax/VE composites are discussed with the XRD results.

3.2 Mechanical Properties

3.2.1 Interfacial Properties

The interfacial properties of flax/VE composites were evaluated by short-beam shear tests. The results of

short-beam shear tests of flax/VE composites are presented in Figure 4 and Table 4 to compare the interlaminar properties of the flax/VE composites. The standard deviation was calculated for each of the samples with a minimum of five specimens. Interlaminar shear strength is a function of fiber to matrix bonding. Higher ILSS values indicate better interfacial adhesion between fiber and matrix. A successful short-beam test is one in which the failure initiates at the interface between fiber and matrix and the tight tolerances should be maintained in the specimen dimensions. Comparing the untreated and treated flax composites, it was observed that both surface treatments on flax and resin manipulations improved the interlaminar shear strength. This implies that both treatments enhanced the adhesion between fiber and matrix.

It was observed that the interlaminar shear strength of treated flax/VE was 226% higher than that of untreated flax/VE and the specific ILSS of treated flax/VE was 216% higher than that of untreated flax/VE. The differences between untreated and treated flax composites are due to the effect of alkaline treatment. Alkaline treatment removes the non-cellulosic chemicals, which provides rough surface of flax, and separates the big fiber bundles into smaller fiber bundles, which increases the contact area between fiber
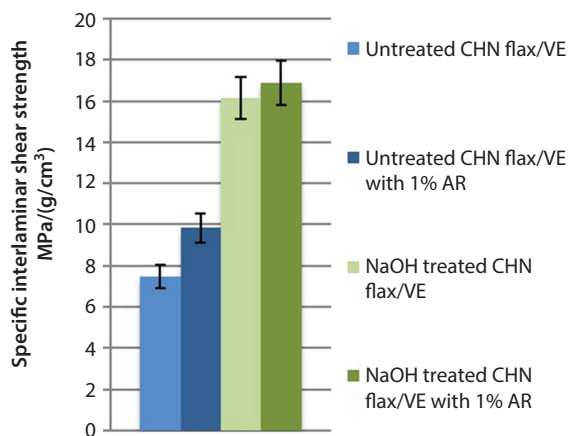
and matrix [22]. All these effects increase the mechanical interlocking between flax and VE. In addition, alkaline treatment exposes more cellulose molecules on the fiber surface, which increases the chances to form hydrogen bonds between cellulose and VE. Both mechanical interlocking and hydrogen bonds can increase the interlaminar shear strength of the composites.

The interlaminar shear strength of treated flax/VE with 1 wt% AR shows slight increases over the treated flax/VE. AR as an additive increases the hydrophilicity of VE system according to the results of moisture absorption and contact angle tests, which can reduce the repulsion between flax and VE. However, there is no evidence that there is any type of chemical bond existing between flax and VE with AR from the FTIR spectra of flax composites [9]. Thus, AR does not introduce or form any chemical bonds with flax to increase the interfacial properties of the composites. The misalignment of fiber bundles in the composites can increase the standard deviation of the tests' results. Moreover, the variation of the fiber volume fraction in different composites introduces some differences in the final results. Therefore, in Figure 3, all results were normalized by composite density.

3.2.2 Tensile Properties

Tensile properties were analyzed to correlate the effects of both fiber loading and processing methodology upon unidirectional flax fiber composites. The results of tensile tests of flax composites are presented in Figure 5 and Table 5. The specific tensile modulus of untreated flax/VE was the lowest, which is similar to its specific tensile strength. It means all the surface treatments and modifications improve the tensile performance of flax/VE composites.

Untreated flax/VE with AR composites perform better than untreated flax/VE in tensile modulus and specific tensile modulus. The specific tensile modulus of untreated flax/VE with 1% AR is shown to be approximately 24% higher than that of untreated flax/VE. It indicates AR additive helps the load transfer between matrix and fiber by increasing the interfacial

Figure 4 Comparison of specific interfacial shear strength of different types of flax/VE composites.

Table 4 Interfacial properties comparison of Chinese flax/VE composites.

Sample	Interlaminar shear strength (MPa)	Density (g/cm³)	Fiber volume fraction (%)
Untreated CHN Flax/VE	9.46±0.69	1.27±0.01	41.72
Untreated CHN Flax/VE with 1% AR	12.63±0.90	1.28±0.02	44.00
EtO⁻Na⁺ treated CHN Flax/VE	21.44±1.35	1.33±0.03	44.28
EtO⁻Na⁺ treated CHN Flax/VE with 1% AR	22.30±1.39	1.3 2±0.02	44.65

interaction between fiber and matrix, which is confirmed by the results of ILSS that AR improves the interfacial properties of flax composites. Moreover, AR additive increases the elastic modulus of VE according to the results from the study of resin system. Thus, the tensile modulus of flax/VE with AR composites can be increased with AR. However, treated flax/VE with 1% AR composites show a similar specific tensile

modulus to that of treated flax/VE, which are all close to the specific tensile modulus of untreated flax/VE with AR composites.

In tensile tests, the properties of flax fiber dominate the tensile performance of their composites. The chemical treatment applied in this study has minimal influence on the properties of flax. The flax fiber bundle structure is varied during the alkaline treatment [23]. Some chemical modifications on the surface of flax can damage fibers, such as the hydrolysation of cellulose during the treatment, which has been proved in previous work [24]. The similarity in specific tensile modulus of modified composite is because of the minimal changes in the flax properties. In addition, the variation of fiber orientation in different composites' panels can affect their mechanical performance. The standard deviation of treated flax/VE with 1% AR was quite large, which indicates the existance of misalignment of flax or voids in their composites.

The trend of the specific tensile strengths of flax composites is similar to the trend of their ILSS and specific flexural modulus. The specific tensile strengths of treated flax composites are higher than those of untreated flax composites. The NaOH/ethanol treated flax/VE performs 67% higher than untreated flax/VE in specific tensile modulus. In addition, the specific tensile strength of NaOH/ethanol flax/VE with 1% AR shows an approximate 135% increase compared to that of untreated flax/VE with 1% AR. These significant increases in specific tensile strength result because alkaline treamtent can change the crystallinity of cellulose [10]. The crystal structure changes of cellulose during alkaline treatment have been proven by the FTIR spectra [8]. On the other hand, the standard deviations of tensile results are in a wide range. The misorientation of flax fiber during the composites' processing can increase the variation of the tests' results. In addition, the fiber volume fraction of different flax composites varied and some of the changes in the composites' density are inconsistent with their fiber volume fraction, which is due to the changes of the voids in the composites.
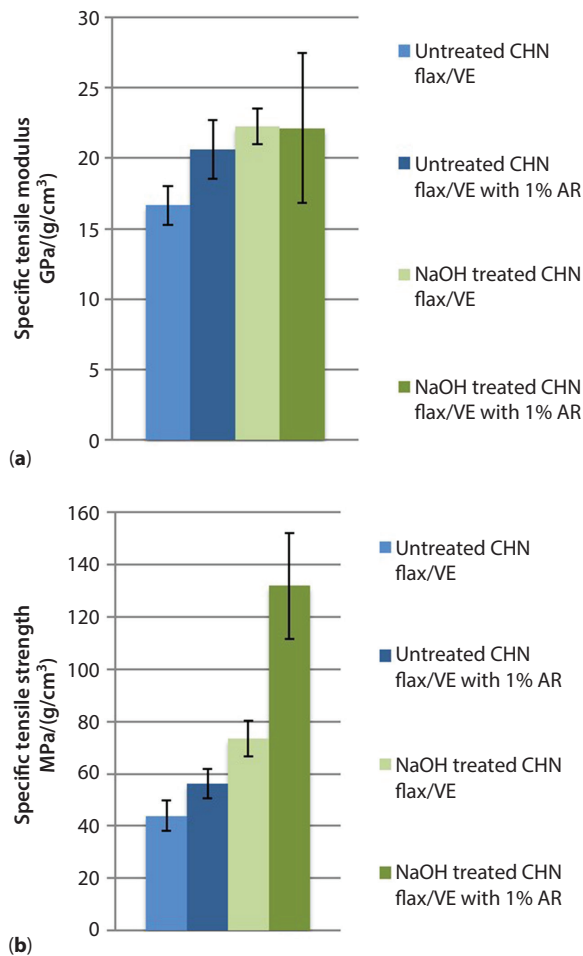

Figure 5 Comparison of specific tensile properties of Chinese flax/VE composites: (**a**) specific tensile modulus and (**b**) specific tensile strength.

Table 5 Tensile properties comparison of Chinese flax/VE composites.

Sample	Tensile modulus (GPa)	Tensile strength (MPa)	Density (g/cm³)	Fiber volume fraction (%)
Untreated CHN Flax/VE	21.13±1.77	55.69±7.48	1.27±0.05	50.34
Untreated CHN Flax/VE with 1% AR	26.14±2.61	71.01±7.18	1.27±0.03	45.71
EtO⁻Na⁺ treated CHN Flax/VE	28.63±1.61	94.39±8.74	1.29±0.07	45.59
EtO⁻Na⁺ treated CHN Flax/VE with 1% AR	29.46±7.09	175.71±26.98	1.33±0.01	46.40

3.2.3 XRD Results

Flax/VE (unmodified and modified) composites containing isolated small spherical filler particles (Al powders) were also prepared. The concentration of Al powder ethanol solution was selected after preliminary experiments. In the preliminary study, 0.1%, 0.3% and 0.5% Al/ethanol slurries were prepared to distribute Al uniformly into alkaline treated flax. The treated flax fibers with Al powder were processed into the composites' panels, which were used for X-ray diffraction. A 0.5% Al/ethanol slurry provided XRD signals, in which the intensity was strong enough to distinguish the small changes of X-ray diffraction angles. On the other hand, the small spherical Al particles in the composites were very small amounts, so the Al powder's contribution to the stress state of the specimen can be neglected. The spherical Al particles were evenly distributed in the flax/VE composites to form the intralaminar composite architecture. The XRD spectra of Al powder in treated flax/VE with 1% AR are from different angles (ϕ and ψ). The direction $\phi = 0°$ was chosen parallel to the fibers' direction and $\phi = 90°$ was the transverse direction. Three ψ angles were selected between 0° to 45° for each ϕ angle. It is observed that the differences of 2θ from (422) plane from different measured angles (ϕ and ψ) are fairly small and the peak separation was carried out by least squares fitting by Gaussian functions. The lattice spacing d_0 for different angles are listed in Table 6, in which the lattice spacings d_0 were calculated using Bragg's law.

Equation 2 can be written as:

$$\sigma_{11} - \sigma_{22} = \frac{1}{\frac{1}{2} S_2^{hkl}} \frac{\partial \varepsilon_{\varphi=0,\psi}}{\partial \sin^2 \psi} \quad (5)$$

where $\dfrac{\partial \varepsilon_{\varphi=0,\psi}}{\partial \sin^2 \psi}$ is the slope of the $\varepsilon_{\varphi = 0, \Psi}$ vs. $\sin^2\Psi$ plot.

When $\varphi = 0$ and Ψ were varied, Equation 2 can also be written as:

Table 6 The lattice spacings of Flax/VE composites at different angles for Al.

Sample	Sin²ψ	d₀ (Å)	
		$\phi = 0°$	$\phi = 90°$
Flax/VE	0.00	0.8269	0.8269
	0.25	0.8268	0.8269
	0.50	0.8268	0.8270
Flax/VE with 1% AR	0.00	0.8270	0.8267
	0.25	0.8269	0.8269
	0.50	0.8268	0.8270

$$\sigma_{22} - \sigma_{33} = \frac{1}{\frac{1}{2} S_2^{hkl}} \frac{\partial \varepsilon_{\varphi=90,\psi}}{\partial \sin^2 \psi} \quad (6)$$

where $\dfrac{\partial \varepsilon_{\varphi=90,\psi}}{\partial \sin^2 \psi}$ is the slope of the $\varepsilon_{\varphi = 90,\Psi}$ vs. $\sin^2\Psi$ plot.

In addition, σ_{33} can be written as:

$$\sigma_{33} = \frac{\dfrac{d_{\varphi=0,\psi=0} - d_0}{d_0} - S_1^{hkl}(\sigma_1 + \sigma_2)}{S_1^{hkl} + \dfrac{1}{2} S_2^{hkl}} \quad (7)$$

The principal strains and principal stresses can be calculated by Equations 5–7. But this method is not valid if the $\varepsilon_{\varphi\psi}$, vs. $\sin^2\Psi$ plots are oscillatory.

X-ray elastic constants (XEC) can be obtained using single crystal elastic constants S_{11}, S_{12} and S_{66} for cubic symmetry. The following equations can be obtained for the Voigt and Reuss models [25] and the average XEC calcuated by Voigt and Reuss models and for Al are presented in Table 7.

The stress and the strain measured at $\phi\psi$ direction can be calculated by Equation 8 and Equation 9:

$$\sigma_{\varphi\psi} = \sigma_{11} \cos^2 \varphi \sin^2 \psi + \sigma_{22} \sin^2 \varphi \sin^2 \psi + \sigma_{33} \cos^2 \psi$$

$$(8)$$

$$\varepsilon_{\varphi\psi} = \varepsilon_{11} \cos^2 \varphi \sin^2 \psi + \varepsilon_{22} \sin^2 \varphi \sin^2 \psi + \varepsilon_{33} \cos^2 \psi \quad (9)$$

The least squares method can be applied to Equation 2 and Equation 3 to obtain least squares values of the principal stresses and principal strains. If there are shear stresses and strains existing in the system, the least squares method can be applied. If there are no shear stresses and strains, the linear squares method can be used. The $\varepsilon_{\varphi\Psi}$ vs. $\sin^2\psi$ plots should be non-oscillatory when this method is applied.

The normal strain ε_{33} was obtained from the average between $\varepsilon_{\phi = 0, \psi = 0}$ and $\varepsilon_{\phi = 0, \psi = 90}$. The least squares method was applied to determine the slope of the line on $\varepsilon_{\phi\psi}$ vs. $\sin^2\psi$ plot. ε_{11} and ε_{22} were calcuated from the slopes of $\varepsilon_{\phi\psi}$ vs. $\sin^2\psi$ plot at $\phi = 0°$ and 90° respectively.

X-ray elastic constants on (422) plane are used to calculate Young's modulus E and Poisson's ratio (ν) values of Al by Equation 10 and Equation 11:

$$S_1 = -\frac{\nu}{E} \quad (10)$$

$$\frac{1}{2} S_2 = \frac{1+\nu}{E} \quad (11)$$

As a result, E is 71 GPa and ν is 0.351. Assuming the material is isotropic, the stresses were calcuated from

Table 7 Single crystal elastic constants and XEC for Al powder.

Inclusion	S_{11} (10^{-3} GPa^{-1})	S_{12} (10^{-3} GPa^{-1})	S_{44} (10^{-3} GPa^{-1})	S_1(hkl) (10^{-3} GPa^{-1})	½ S_2(hkl) (10^{-3} GPa^{-1})
Al (422)	15.8	-5.8	35.8	-4.9	19.0

Table 8 Strains and stresses inside Al powders.

Sample	ε_{11} (10^{-6})	ε_{22} (10^{-6})	ε_{33} (10^{-6})	σ_{11} (MPa)	σ_{22} (MPa)	σ_{33} (MPa)
Al in Flax/VE	719.86	−547.12	31.85	50.50	−16.09	14.34
Al in Flax/VE with 1% AR	374.54	−327.06	47.38	25.56	−11.31	8.36

the strains by generalized Hooke's law. Table 8 presents the strains and stresses inside Al inclusions.

There are no external stresses applied on the composite, so the stresses inside the Al inclusion are related to the thermal residual stresses generated by the matrix. It can be seen that the residual stress depends on both matrix and the inclusion properties and the residual strain due to the thermal expansion misfitting can be expressed as:

$$\varepsilon^T = \left(\alpha_M - \alpha_i \right) \Delta T \tag{12}$$

where α_M stands for the coefficient of thermal expansion of the matrix, α_i is the coefficient of thermal expansion of the inclusion, and $(\alpha_M - \alpha_i)$ depends on the direction.

After obtaining the stress state inside the Al inclusion, the stresses in matrix can be assessed. Eshelby's inclusion theory is one of the most often applied theoretical methods to evaluate the stresses in matrix. In the Eshelby model, the ellipsoidal inclusions are randomly distributed within the matrix and the stress in the inclusion is uniform. Using the condition of microstress balance expressed in Equation 13,

$$\left(1 - f \right) < \sigma_M > + f < \sigma_I > = 0 \tag{13}$$

where f is the fraction of inclusion I in a matrix M. Using the principal of equivalent inclusion and traction forces at the interfaces, the stresses generated from matrix can be calculated. The stress transfer factors as a matrix with three components along the first diagonal should be considered.

$$\sigma_{Al} = \kappa \sigma_M \tag{14}$$

where

$$k = \begin{bmatrix} k_{11} & 0 & 0 \\ 0 & k_{22} & 0 \\ 0 & 0 & k_{33} \end{bmatrix} \tag{15}$$

The stress transfer factors are related to the properties of matrice and inclusions. Assuming the matrix is homogeneous and isotropic, Hauk [26] gave the

figures which provide the relation between stress transfer factor vs. logarithm of the ratio of Young's moduli $\log(E_{matrix}/E_{inclusion})$. According to the figures [22], is 1.9, are −0.3. The stresses from VE matrices can be calculated by Equation 14. The strains in matrix were calculated by generalized Hooke's law. Table 9 lists the stresses and strains from both VE and VE with 1% AR. In the next section, the effects of these stresses and strains in the matrix are discussed.

3.3 Residual Stresses in Flax/VE Composites

The stresses calculated in the Al powder are assumed to be equivalent to the residual stresses in the matrix generated by the curing, which are equivalent to the results in Table 9. Thus, the principal residual stresses and strains in different VE systems are equivalent to the values listed in Table 9. It was observed that the residual stresses $\sigma_{11}{}^R$ and $\sigma_{22}{}^R$ in VE with 1% AR are lower compared to those residual stresses in neat VE system. Residual stress $\sigma_{11}{}^R$ is parallel to the longitudinal direction of the flax fiber, which is not related to the interface between fibers and matrix. Resisual stress $\sigma_{22}{}^R$ is one of the transverse directions, which is related to the misfitting of thermal expansion between flax and VE matrix. Residual stress $\sigma_{33}{}^R$ is not only generated by the thermal expansion in the composites, but is also related to the external loading during the processing of the composites' panels. Moreover, the external force applied on 33 direction is about 1 metric ton, which introduces a large influence on $\sigma_{33}{}^R$. Thus, $\sigma_{22}{}^R$ is the one which can explain the relationship between thermal residual stresses and interfacial adhesion in the flax/VE composites. These residual stresses are related to the interaction between VE and Al inclusions and are the local stresses around Al. Accordingly, the residual stresses around flax fiber are determined by the interaction between flax and VE.

The coefficient of thermal expansion of cured VE system is increased by AR additive, which is 21.46 µm/m °C. The CLTE of Al inclusion is 22.4 µm/m °C and is close to CLTE of modified VE system.

Table 9 Stresses and strains from VE and VE with 1% AR.

Sample	σ_{11} (MPa)	σ_{22} (MPa)	σ_{33} (MPa)	ε_{11} (10^{-6})	ε_{22} (10^{-6})	ε_{33} (10^{-6})
VE in Flax/VE	26.58	53.63	−47.79	0.023	0.058	−0.075
VE in Flax/VE with 1% AR	13.45	37.72	−27.87	0.0075	0.034	−0.038

It is known that the thermal residual stresses are generated by the mismatching of CTEs of VE and Al inclusion. The increase in CLTE of modified VE reduces the difference in thermal expansion/contract between VE and Al inclusion. Thus, both residual stresses σ_{11}^R and σ_{22}^R in VE with 1% AR exhibit a decrease compared to neat VE system.

The CLTE of treated flax in transverse direction is −299.1 μm/m °C, which was measured by TMA. Flax fibers shrink in transverse direction when the temperature rises, which is opposite to VE resin and Al inclusion. Thus, AR additive actually further enlarges the difference of CLTE between VE and flax in transverse direction. There are three steps in the curing process of VE system. In the first step, the initiator (peroxide) generates the free radicals to start the polymerization in VE resin. The second step is the growth of the polymer chains, in which the temperature of the system starts to rise because this chemical reaction is an exothermic process. The third step is the termination of the chains' growth and the temperature of VE system is still much higher than room temperature. After VE is cured, the temperature of the composite panel starts to decrease to the room temperature. During the cooling process, VE matrix starts to shrink in all directions and flax fiber begins to expand in transverse directions. The thermal behaviors of flax fiber and VE on the interface during the cooling are sketched in Figure 6. The blue arrows indicate the direction of the expansion of flax fiber during the cooling and the red arrows stand for the direction of the contraction of VE.

The changes of residual stresses in unmodified and modified VE at the local area surrounding Al inclusion were discussed. The AR additive increases the CLTE of modified VE system and reduces the mismatching between VE and Al inclusion, which causes the reduction of residual stresses in the matrix. It helps to predict that the residual stresses in the matrix around flax fibers increases in the modified VE. The residual stresses in the matrix around flax fibers should decrease in tension or increase in compression in transverse direction. As Figure 6 shows, the local stresses on the interface of flax VE should be compressive in nature, generated by the thermal expansion/contraction behavior. These thermal residual compressive stresses push flax fibers and VE matrix towards each other and increase the mechanical interlocking, which improves the interfacial interaction between flax and VE.
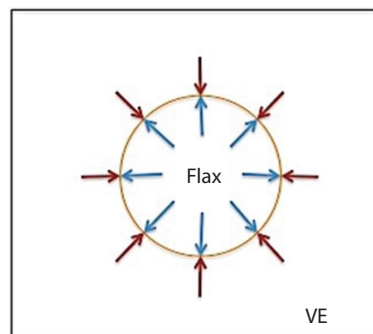
Figure 6 The thermal behaviors of flax and VE on the interface.

The AR additive increases the coefficient of thermal expasion of VE, which enlarges the thermal contraction of VE system during the cooling. The compressive stresses on the interface of flax/VE with AR composites can also increase, which causes stronger mechanical interlocking between flax and VE. The interlaminar shear strength and elastic moduli of flax/VE with AR composites are higher and therefore confirm the improvement on the interfacial adhesion between flax and VE. However, the interfacial properties of flax/VE composites in this study are discussed at room temperature. If the specimens are tested at an elevated temperature, the interfacial properties of flax/VE composites should decrease because of the decrease of thermal residual stresses in transverse direction.

Considering the effects of the coefficients of thermal expansion of flax and VE system, it is easy to predict the mechanical interaction between flax and VE on the interface of their composites. By changing CLTE of VE, the interfacial adhesion of flax/VE composites can be improved. There are several methods to measure the coefficient of thermal expansion of VE system and they are simple and cost saving. They provide a direction from the mechanical aspect to manipulate resin system to enhance the interfacial properties of the flax composites.

On the other hand, if both the reinforced fiber and polymer matrix contract with the decrease of temperature (Figure 7), increasing the coefficient of thermal expansion of polymer matrix to generate compressive thermal residual stresses can also improve the interfacial properties of their composites. If both the reinforced fiber and polymer matrix
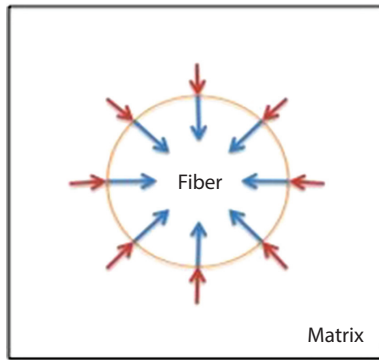
Figure 7 The thermal behaviors of fiber and polymer matrix on the interface.

expand with the decrease of temperature, reducing the CLTE of polymer matrix to produce compressive thermal residual stresses can improve the interfacial interaction of its composites. However, this method is constricted by the application temperature of the composites.

4　CONCLUSIONS

In this work, the coefficients of the linear thermal expansion of flax and different VE systems were evaluated. The study of residual stresses in the composites by X-ray diffraction technique provided a new method to evaluate the interfacial properties of cellulosic composites and shows the effects of thermal expansion/contraction of both fiber and resin on their interfacial adhesion. There are many studies which show how chemical bonding, wettability and processing methods influence the mechanical performance of cellulosic fiber composites. However, this is the first time the thermal properties of flax and VE were taken into account to analyze the interfacial properties. This provides a more comprehesive understanding about the physical factors which can affect the interfacial properties of unidirectional cellulosic fiber reinforced thermoset composites.

The theory of changing (increasing or reducing) the coefficient of thermal expansion of VE system by adding AR can be applied to other thermoset resin systems. With the knowledge of the thermal properties of cellulosic fiber and resin system, a low-cost, time-efficient modification method can be easily developed.

For future work, thermal properties of other cellulosic composites should be investigated. With enough experimental results on thermal properties and interfacial properties, the theoretical model between the thermal properties and interfacial properties in the cellulosic fiber composites could be developed. Finally, the study of the moisture resistance of cellulosic

composites should be investigated because it plays an important rule in the application and service life of cellulosic composites.

ACKNOWLEDGMENTS

REFERENCES

1. E. Kvavadze, O. Bar-Yosef, A. Belfer-Cohen, E. Boaretto, N. Jakeli, Z. Matskevich, and T. Meshveliani, 30,000-Year-Old Wild Flax Fibers. *Science* **325**, 1359 (2009).
2. M. Ragoubi, D. Bienaime, S. Molina, B. George, and A. Merlin, Impact of corona treated hemp fibres onto mechanical properties of polypropylene composites made thereof. *Ind. Crop. Prod.* **31**, 344–349 (2010).
3. A.C. Milanese, M.O.H. Cioffi, and H.J.C. Voorwald, Mechanical behavior of natural fiber composites. *Procedia Eng.* **10**, 2022–2027 (2011).
4. A. Singha and R. Rana, Chemically induced graft copolymerization of acrylonitrile onto lignocellulosic fibers. *J. Appl. Polym. Sci.* **124**, 1891–1898 (2012).
5. S. Alix, L. Lebrun, S. Marais, E. Philippe, A. Bourmaud, C. Baley, and C. Morvan, Pectinase treatments on technical fibre of flax: Effects on water sorption and mechanical properties. *Carbohydr. Polym.* **87**, 177–185 (2012).
6. X. Li, L. He, H. Zhou, W. Li, and W. Zha, Influence of silicone oil modification on properties of ramie fiber reinforced polypropylene composites. *Carbohydr. Polym.* **87**, 2000–2004 (2012).
7. T.E. Motaung, M.E. Mngomezulu, and M.J. Hato, Effects of alkali treatment on the poly(furfuryl) alcohol–flax fibre composites. *J. Thermoplast. Compos. Mater.* DOI: 10.1177/0892705716679478 (2016).
8. S. Huo, V.S. Chevali, and C.A. Ulven, Study on interfacial properties of unidirectional flax/vinyl ester composites: Resin manipulation on vinyl ester system. *J. Appl. Polym. Sci.* **128**(5), 3490–3500 (2013). DOI: 10.1002/app.38565
9. S. Huo, The physico-chemical investigation of interfacial properties in natural fiber/vinyl ester biocomposites. PhD Dissertation, NDSU (2012).
10. M.Z. Rong, M.Q. Liu, Y. Liu, G.C. Yang, and H.M. Zeng, The effect of fiber treatment on the mechanical properties of unidirectional sisal-reinforced epoxy composites. *Compos. Sci.* **61**, 1437–1447 (2001).
11. Y. Cao, D. Yu, L. Chen, and J. Sun, Internal stress of modified epoxy resins with polyester. *Polym. Test.* **20**, 685–692 (2001).

12. B. Zhang, Z. Yang, and X. Sun, Measurement and analysis of residual stresses in single fiber composite. *Mater. Design* **31**, 1237–1241 (2010).

13. F. Naya, J.M. Molina-Aldareguia, C.S. Lopes, C. Gonzalez, and J. Lloraca, Interface characterization in fiber-reinforced polymer–matrix composites. *JOM* **69**, 13–21 (2017).

14. P.P. Parlevliet, H.E.N. Bersee, and A. Beukers, Residual stresses in thermoplastic composites – a study of the literature – part I: Formation of residual stresses. *Compos. Part A* **37**, 1847–1857 (2006).

15. N.H. Mostafa, Z.N. Ismarrubie, S.M. Sapuan, and M.T.H. Sultan, Fibre prestressed polymer-matrix composites: A review. *J. Compos. Mater.* **51**, 39–66 (2016).

16. M.G.R. Sause, *In Situ Monitoring of Fiber-Reinforced Composites: Failure of Fiber-Reinforced Composites*, pp. 5–55, New York, Springer International Publishing (2016).

17. A. Mustata, Factors influencing fiber-fiber friction in the case of bleached flax. *Cell. Chem. Technol.* **31**, 405–413 (1997).

18. K. Shivakumar and A. Bhargava, Failure mechanics of a composite laminate embedded with a fiber optic sensor. *J. Compos. Mater.* **39**, 777–798 (2005).

19. B. Benedikt, M. Kumosa, P.K. Predecki, L. Kumosa, M.G. Castelli, and J.K. Sutter, An analysis of residual thermal stresses in a unidirectional graphite/PMR-15 composite based on X-ray diffraction measurements. *Compos. Sci.* **61**, 1977–1994 (2001).

20. H. Dölle, The influence of multiaxial stress states, stress gradients and elastic anisotropy on the evaluation of (residual) stresses by X-rays. *J. Appl. Crystallogr.* **12**, 489–501 (1979).

21. V. Hauk, Structural and residual stress analysis by X-ray diffraction on polymeric materials and composites. *Adv. X-Ray Anal.* **42**, 540–554 (2000).

22. M.A. Fuqua, S. Huo, and C.A. Ulven, Natural fiber reinforced composites. *Polym. Rev.* **52**, 259–320 (2012).

23. M. Schwanninger, J.C. Rodrigues, H. Pereira, and B. Hinterstoisser, Short-time vibratory milling of wood and cellulose: Effects on the shape of FT-IR spectra. *Vib. Spectrosc.* **36**, 23–40 (2004).

24. W.A. Jensen, *Botanical Histochemistry – Principles and Practice*, University of California, Berkeley, W.H. Freeman and Company (1962).

25. C.S. Barrett and P. Predecki, Stress measurements in graphite/epoxy uniaxial composites by X-rays. *Polym. Compos.* **1**, 2–6 (1980).

26. V. Hauk, *Structural and Residual Stress Analysis by Nondestructive Methods*, pp. 129–215 and 279–336, Amsterdam, Elsevier Science B.V. (1997).